Validation of MODIS integrated water vapor product against reference GPS data at the Iberian Peninsula

Javier Vaquero-Martínez[1], Manuel Antón

Departamento de Física, Universidad de Extremadura, Badajoz (Spain)

Instituto Universitario de Investigación del Agua, Cambio Climático y Sostenibilidad (IACYS), Universidad de Extremadura, Badajoz (Spain)

José Pablo Ortiz de Galisteo

Agencia Estatal de Meteorologia (AEMET), Valladolid (Spain)

Grupo de Óptica Atmosférica, Universidad de Valladolid, Valladolid (Spain)

Victoria E. Cachorro

Grupo de Óptica Atmosférica, Universidad de Valladolid, Valladolid (Spain)

Maria João Costa

Departamento de Física, Instituto de Ciências da Terra, Escola de Ciências e Tecnología, Universidade de Évora, Évora, (Portugal)

Roberto Román

Department of Applied Physics, University of Granada, Granada (Spain)

Andalusian Institute for Earth System Research (IISTA-CEAMA), Granada (Spain)

Yasmine S. Bennouna

Grupo de Óptica Atmosférica, Universidad de Valladolid, Valladolid (Spain)

Abstract

In this work, the water vapor product from MODIS (MODerate-resolution Imaging Spectroradiometer) instrument, on-board Aqua and Terra satellites, is compared against GPS water vapor data from 21 stations in the Iberian Peninsula as reference. GPS water vapor data is obtained from ground-based receiver stations which measure the delay caused by water vapor in the GPS microwave signals. The study period extends from 2007 until 2012. Regression analysis

[1]javier_vm@unex.es

in every GPS station show that MODIS overestimates low integrated water vapor (IWV) data and tends to underestimate high IWV data. R^2 shows a fair agreement, between 0.38 and 0.71. Inter-quartile range (IQR) in every station is around $30\% - 45\%$. The dependence on several parameters was also analyzed. IWV dependence showed that low IWV are highly overestimated by MODIS, with high IQR (low precision), sharply decreasing as IWV increases. Regarding dependence on solar zenith angle (SZA), performance of MODIS IWV data decreases between $50° - 90°$, while night-time MODIS data (infrared) are quite stable. The seasonal cycles of IWV and SZA cause a seasonal dependence on MODIS performance. In summer and winter, MODIS IWV tends to overestimate the reference IWV value, while in spring and autumn the tendency is to underestimate. Low IWV from coastal stations is highly overestimated ($\sim 60\%$) and quite imprecise (IQR around 60%). On the contrary, high IWV data show very little dependence along seasons. Cloud-fraction (CF) dependence was also studied, showing that clouds display a negligible impact on IWV over/underestimation. However, IQR increases with CF, except in night-time satellite values, which are quite stable.

Keywords: MODIS, water vapor, validation, IWV, GPS, satellite.

---

1. Introduction

Water vapor is the most important atmospheric greenhouse gas, and its phase changes involve exchanges of latent heat energy. Water is evaporated at low latitudes, and its vapor is transported towards higher latitudes to condensate, releasing high amounts of heat (Myhre et al., 2013). Moreover, it is well known that water vapor involves a positive feedback in climate change, according to general circulation models (Colman, 2003). Usually, water vapor is quantified using the column integrated amount of atmospheric water vapor (IWV), which is equivalent to condensing all the water vapor in the atmospheric column and measuring the height that it would reach in a vessel of unit cross section; IWV can be measured in columnar mass density (g/cm^2 or kg/m^2) or

in length (height) units (mm).

Some details about the role of water vapor in the atmosphere are still to be completely understood. Thus, it is necessary to monitor water vapor, but this is not a trivial issue for two reasons: the first one is its high variability, both temporal and spatial. Water vapor exhibits both an annual (Ortiz de Galisteo et al., 2014) and diurnal (Ortiz de Galisteo et al., 2011) cycle; therefore, good temporal resolution is very important in water vapor monitoring, especially for some applications. The second reason is that the world coverage is not homogeneous. Water vapor data is scarce over polar and oceanic regions, due to the lack of ground-based observations. Over land, there is still some scarcity over some parts of Africa, South America, and North Asia (see Wang et al., 2007).

There are several instruments for measuring IWV: micro-wave radiometers (Turner et al., 2007), star-photometers (Pérez-Ramírez et al., 2012), moon-photometers (Barreto et al., 2013), sun-photometers (Ichoku et al., 2002), lidar (Turner et al., 2002), GPS system (Ortiz de Galisteo et al., 2011), radiosounding (Torres et al., 2010). Additionally, numerous instruments on board satellite platforms can also retrieve IWV data using different parts of the electromagnetic spectrum: microwave by MLS (Livesey & Van Snyder, 2004) and SSM/I (Wentz & Spencer, 1998)); visible by GOME-2 (Grossi et al., 2015), OMI (Wang et al., 2014) and SCIAMACHY (Noël et al., 2004); near infra-red by MODIS (Gao & Kaufman, 1992; Gao & Li, 2008), and infra-red by MODIS (Seemann et al., 2006), AIRS (Barnet et al., 2007), AMSR-E (Wentz & Meissner, 2007) and SEVIRI (Schroedter-Homscheidt et al., 2008; Martinez, 2013).

Radiosounding and GPS are among the most powerful techniques to study IWV. However, temporal resolution of radiosounding is generally limited to one or two measurements per day. In contrast, GPS provides a high temporal resolution with numerous records throughout the day-time and night-time. Hence, GPS measurements of water vapor have been validated, as in Wang et al. (2007) (against radiosonde, microwave radiometer and satellite data), Ohtani & Naito (2000) (against radiosonde), Bokoye et al. (2003) (against radiosonde

and radiometer), Heise et al. (2009) (against ECMWF reanalysis), Schneider et al. (2010) (intercomparison with spectrometer, radiometer and sunphotometer, and radiosondes), and Pany et al. (2001) and de Haan et al. (2002) (tested against a numerical model). From all these validation exercises, GPS IWV data have been checked as a reliable reference, with bias around 2 mm and standard deviation of about 1.22 mm (see Wang et al., 2007).

GPS measurements of water vapor, however, have two relevant drawbacks. First, ground-based stations are necessary, so coverage is limited to land areas. Second, spatial resolution depends on density of the networks available. Some applications, such as weather forecasts and climate studies, need higher spatial resolution to represent properly the high spatial variability of water vapor. Satellite retrievals have, however, some issues. On the one hand, polar orbiting satellites have a low temporal coverage (one or two measurement a day, usually) depending on the latitude of the area and the swath width of the satellite. On the other hand, visible or NIR radiation is usually used, making cloudy-scene measurements unreliable due to the opacity of clouds.

This work aims to validate data from MODIS satellite radiometer against reference GPS network in the Iberian Peninsula. MODIS data have been validated before (Li et al., 2003; Gao & Li, 2008; Prasad & Singh, 2009; Chang et al., 2015; Ningombam et al., 2016) in other areas. However, over the Iberian Peninsula, MODIS has only been validated in Bennouna et al. (2013); Román et al. (2014). This paper aims to study the dependence of several parameters - IWV, solar zenith angle (SZA), seasonality and clouds - on MODIS performance, which has never been done before to our knowledge. Therefore, it is expected that this paper will contribute to understand the main drawbacks of the IWV product derived from MODIS, allowing the comparison with other regions and possible improvements for the retrieval algorithm.

2. Instruments and Data

2.1. MODIS

MODIS is a radiometer on board Terra (launched in 1999) and Aqua (launched in 2002) satellite platforms (Salomonson et al., 1989; King et al., 1992). Both platforms are sun-synchronous, polar-orbiting satellites, covering the whole planet in 1-2 days. Terra's orbit around the Earth is scheduled to overpass the equator from north to south in the morning, while Aqua passes from south to north over the equator in the afternoon. MODIS swath width is 2330 km.

MODIS measures in 36 spectral bands, covering the range $0.4\ \mu\text{m} - 15\ \mu\text{m}$ acquiring data at three spatial resolutions - 250, 500, and 1000 m. However, level 2 moisture profiles and IWV are derived for 5×5 pixels, which have 1 km^2 resolution, thus, the resolution of the IWV product is 5 km $\times$ 5 km.

Water vapor is generated for both daytime and night. For daytime five NIR bands (channels 2, 5, 17, 18, 19) are used (solar radiation reflected by Earth + atmosphere), and for nighttime only IR bands are used (radiation emitted by Earth + atmosphere).

NIR algorithm uses 2-channel and 3-channel rationing techniques, generating look-up tables with values of these ratios and total amount of water vapor associated with such values, using radiative transfer algorithms. Once the total amount of water vapor is obtained, it can be converted to IWV taking into account the solar and observational geometries. In the presence of clouds, other channels in the $0.8 - 2.5\ \mu$m region are used, since they contain information about absorptions due to water vapor above and within clouds. More detailed information about the algorithm can be found in Gao & Kaufman (1992); Gao & Li (2008).

IR algorithm consists on a statistical synthetic regression with a subsequent nonlinear physical retrieval that iteratively improves the MODIS solution fit. It uses 25-36 bands, covering the spectral region between $3 - 14.5\ \mu$m. More details can be found in Seemann et al. (2006).

The data are included in the water vapor product (MOD05_L2 and MYD05_L2)

collection 6. It is, however, obtained from the MODIS Atmospheric Profile (MOD07 and MYD07) Collection 6 product, and then appended to MOD05 product for convenience. MODIS cloud fraction (CF) data has been used as well to select clear-sky scenes and to study cloudiness dependence.

2.2. GPS IWV data

GPS stations can be used to derive atmospheric water vapor products. The method is explained in the following lines, although a more thorough description can be found in Bevis et al. (1992). The strategy used to determine the position of a receiver deals with the measurement of the time spent by the microwave signal on reaching the receiver at GPS station. However, the signal suffers a series of delays along its path. Among them, the delay caused by the tropospheric gases is called Slant Tropospheric Delay (STD). Zenith Tropospheric Delay (ZTD), which is the delay that the signal would have if the GPS satellite was exactly at the station's zenith, can be computed from the STD using the mapping functions (Niell, 2000). Once ZTD is computed, it can be separated into two different contributions: Zenith Hydrostatic Delay (ZHD) and Zenith Wet Delay (ZWD). The former is due to tropospheric gases while the latter is caused by water vapor's dipolar momentum. If surface pressure is known, ZHD can be modeled, and thus ZWD obtained. Then, IWV can be obtained from ZWD if surface temperature and pressure are known.

In this work, ZTD from 21 GPS ground-based stations were used to obtain IWV products (see Figure 1 and Table 1). Tropospheric products (ZTD) were provided by Spanish Geographic Institute "Instituto Geográfico Nacional", which is a local analysis center for the European Reference Frame (EUREF). The meteorological variables (surface pressure and temperature) needed to retrieve IWV from ZTD products were provided by the Spanish Meteorological State Agency (AEMet). Data are interpolated to the time of GPS measurements (one measurement per hour). In the case of temperature (hourly data), data were interpolated linearly, but in the case of pressure (4 data per day) the barometric tide needed to be accounted for. This resulted in an IWV data-set for the

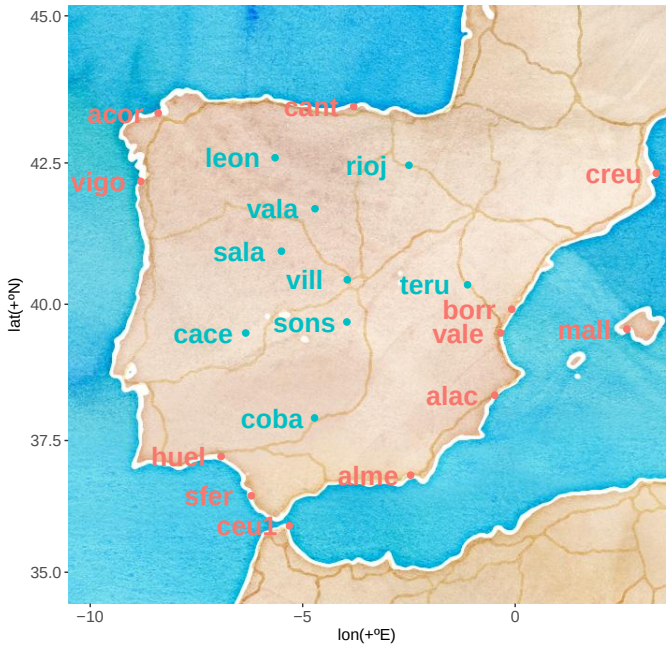

Figure 1: Location of the twenty-one stations selected. Coastal stations are in red and inland stations in blue.

twenty-one GPS stations in the period 2007-2012. Every row in this data-set has several columns: site, date, hour, IWV, CF, SZA, and other columns for additional information.

These data have been used to perform other validation exercises on IWV data from OMI (Vaquero-Martínez et al., 2017), GOME-2 (Román et al., 2015), and MODIS (Bennouna et al., 2013).

3. Methodology

3.1. Comparison criteria

In order to match GPS data and MODIS data, some criteria were applied. First, the distance between the center of the satellite pixel and the ground-based GPS station had to be the lowest. Second, time difference between both measurements had to be the lowest, and always lower than 30 minutes. Otherwise,

the measurement was rejected for this study. Only cloud-free (CF=0) data have been used, except for the analysis on CF dependence, where the whole data-set have been considered.

3.2. Statistical analysis

Once data from MODIS and GPS are co-located according to the criteria mentioned above, a data-set is built, with every row containing a MODIS IWV datum, a GPS IWV datum, SZA, date, CF, and so on. The relative differences between MODIS and GPS are calculated as:

$$\delta_i = 100 \frac{w_i^{\mathrm{MODIS}} - w_i^{\mathrm{GPS}}}{w_i^{\mathrm{GPS}}}$$

where the index i represents a specific location and date, w is the IWV measured by MODIS or GPS. Two indices are applied to the distribution of relative differences: the pseudomedian ($\bar{\delta}$) and the interquartile range (IQR). The pseudomedian is calculated through Wilcoxon signed rank test with continuity correction (Wilcoxon, 1945).

The pseudomedian agrees with the median in a symmetric data-set, and it is defined as the median of all the midpoints of pairs of observations. This has information about the accuracy of the MODIS IWV data. Pseudomedian values close to zero indicate that MODIS and GPS agree well, but positive values of pseudomedian would show that MODIS is overestimating IWV. Negative values, therefore, would be signals of underestimation.

IQR is the difference between the first and the third quartile of the relative differences, which gives the width of the central half of the data. IQR allows measuring the precision of MODIS IWV product.

A statistical analysis per station has been performed in this context, in order to detect differences between stations. In the analysis, both indices (pseudomedian and IQR) over each station have been calculated, and a linear regression model has been applied to the MODIS (dependent variable) and GPS (independent variable) IWV data, in order to analyze their proportionality an similarity.

In order to study the influence of other parameters (SZA, IWV, season and CF), data were binned for these variables, and the indices are calculated over those bins of data. Then, the indices are plotted against the variables. The bin widths have been the following: 5 mm (IWV), 5° (SZA), one month (season), and 0.1 (CF). Bins with few data (less than 30) have been ignored in this paper.

4. Results and discussion

4.1. Statistical analysis

A statistical analysis per stations was performed, whose results can be seen in Table 2. Pseudomedian values show that some stations tend to overestimate reference GPS data, while others tend to underestimate them. However, there is not a clear pattern. IQR, is quite homogenous, with values between 30 and 45%, which shows that MODIS variability is high. This result is similar to that obtained for OMI IWV product in Vaquero (2017). Regarding regression parameters, the intercept, y_0, varies from 0.4 mm to 6.8 mm between stations, but in all cases the intercept is positive, suggesting that low IWV values are probably overestimated by MODIS product. Coastal stations tend to have higher intercepts than inland stations. The slope b, on the contrary, is lower than 1 in all cases (except for *mall*, which is slightly higher than 1). This shows that high IWV values are prone to be underestimated by MODIS. Pearson's coefficient, R^2, indicates a fair agreement between the data, with values from 0.38 to 0.71. In Li et al. (2003), regression between MODIS daytime (NIR) and GPS IWV in Germany showed slopes greater than 1 and intercepts below 0 mm. As it will be mentioned in Section 4.3, MODIS daytime algorithm seems to overestimate IWV with respect to GPS products, which could be the cause for the difference between the results in the present work and those in Li et al. (2003). However, in Ningombam et al. (2016), the results of the regression of MODIS NIR product against GPS measurements of IWV at the dry (IWV typically between $1 - 16$ mm) trans-Himalayan region were quite similar to those in Table 2, as well as in Raja et al. (2008) in north America. In such work the correlation

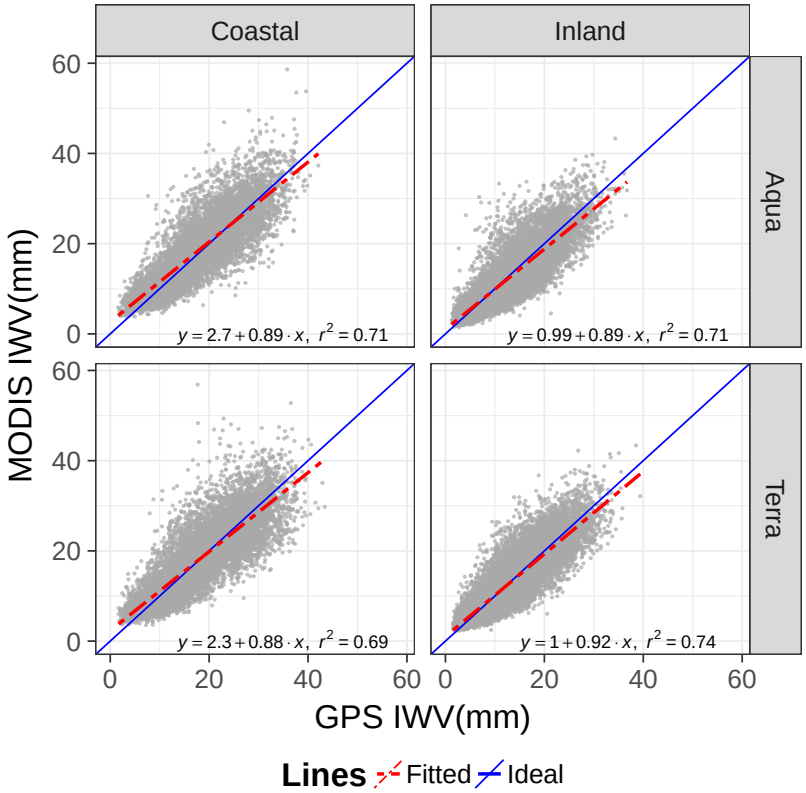

Figure 2: Scatterplot between MODIS retrieved IWV data and GPS IWV data. Data is divided into coastal and inland stations, and into Terra or Aqua data.

between MODIS and GPS were very high, around $R^2 = 0.91$, which could be due to the smaller range of measurement and the selection of good quality data.

Figure 2 shows the scatterplot between MODIS and GPS IWV data. It can be observed that both data sets agree well, better for inland stations and Terra platform. Coastal stations tend to have more dispersion, probably due to the presence of water in the pixels of MODIS, which makes the retrieval more challenging. Furthermore, the better performance of Terra could be due to its typical passing hours (in the morning).

Station	Acronym	Latitude ($^\circ N$)	Longitude ($^\circ E$)	Altitude km
A_Coruña	acor	43.36	-8.40	0.01
Santander	cant	43.47	-3.80	0.05
Vigo	vigo	42.18	-8.81	0.03
Córdoba	coba	37.92	-4.72	0.16
León	leon	42.59	-5.65	0.92
Logroño	rioj	42.46	-2.50	0.45
Salamanca	sala	40.95	-5.50	0.80
Sonseca	sons	39.68	-3.96	0.76
Teruel	teru	40.35	-1.12	0.96
Valladolid	vala	41.70	-4.71	0.77
Villafranca	vill	40.44	-3.95	0.60
Alicante	alac	38.34	-0.48	0.01
Almería	alme	36.85	-2.46	0.08
Burriana	borr	39.91	-0.08	0.02
Ceuta	ceu1	35.89	-5.31	0.05
Creus	creu	42.32	3.32	0.08
Mallorca	mall	39.55	2.63	0.06
Valencia	vale	39.48	-0.34	0.03
Cáceres	cace	39.48	-6.34	0.38
Huelva	huel	37.20	-6.92	0.03
San_Fernando	sfer	36.46	-6.21	0.04

Table 1: Location of GPS stations considered

Station	pMedian (%)	IQR (%)	N	y_0 (mm)	b	R^2
acor	1(1)	39.89	6021	3.4(0.37)	0.79(0.02)	0.49
cant	-9(1)	37.91	5378	3.5(0.36)	0.70(0.02)	0.50
vigo	3(1)	40.82	6673	4.0(0.34)	0.78(0.02)	0.50
alac	2(1)	35.84	6902	2.7(0.36)	0.89(0.02)	0.60
alme	-11(1)	31.52	7342	1.3(0.33)	0.84(0.02)	0.58
borr	-3(1)	30.87	5698	2.1(0.30)	0.86(0.01)	0.71
ceu1	4(1)	42.15	5116	6.8(0.46)	0.66(0.02)	0.38
creu	5(1)	41.03	6080	4.9(0.28)	0.73(0.02)	0.61
mall	12(1)	35.94	6668	1.9(0.39)	1.04(0.02)	0.65
vale	-7(1)	32.89	6669	2.7(0.30)	0.78(0.01)	0.64
huel	14(1)	40.79	6572	4.2(0.39)	0.89(0.02)	0.52
sfer	18(1)	45.10	4496	5.1(0.50)	0.87(0.03)	0.46
coba	-9(1)	30.39	6876	0.9(0.31)	0.87(0.02)	0.62
leon	-2(1)	41.09	6042	1.0(0.22)	0.90(0.02)	0.62
rioj	-15(1)	32.79	5496	0.4(0.25)	0.83(0.02)	0.68
sala	3(1)	41.04	6522	1.1(0.24)	0.95(0.02)	0.63
sons	17(1)	43.03	6288	1.1(0.26)	1.09(0.02)	0.68
teru	-5(1)	38.52	4787	0.8(0.26)	0.90(0.02)	0.66
vala	-4(1)	36.36	5206	0.4(0.28)	0.95(0.02)	0.66
vill	-3(1)	34.00	6683	0.5(0.24)	0.95(0.02)	0.68
cace	12(1)	39.78	6842	1.8(0.29)	1.00(0.02)	0.61
All	0.9(0.7)	39.36	128357	2.3(0.07)	0.870(0.004)	0.61

Table 2: MODIS statistical analysis. The pseudomedian and IQR of the δ distribution, the number of data (N) and the coefficients of the regression analysis are shown. y_0 column shows the intercept, b stands for the slope and R^2 is Pearson's coefficient of determination. The numbers in parenthesis are the 95% confidence interval. The double line separates coastal (top) and inland (bottom) stations.

4.2. IWV dependence

As mentioned above, in order to study IWV dependence, data were grouped in bins of 5 mm, and pseudomedian and IQR were calculated for each bin. In Figure 3 top, it can be observed that low IWV is clearly overestimated, but the rest of IWV are quite close to the zero line, being slightly underestimated. Coastal stations have a slight tendency to overestimation, except for large IWV (IWV $>$ 25 mm), which is underestimated and small IWV (IWV $<$ 10 mm), which is significantly overestimated. Daylight subset pseudomedians are always above nighttime ones. Overestimating daylight (NIR) product has been observed in other studies, such as Albert et al. (2005); Bennouna et al. (2013). Moreover, IQR dependence on IWV, shown in Figure 3 bottom, clearly decreases with increasing IWV. Differences between daytime and nighttime measurements are small (daylight shows a slightly lower IQR than nighttime). Coastal and inland stations behave very similarly, but coastal stations' IQR is generally higher.

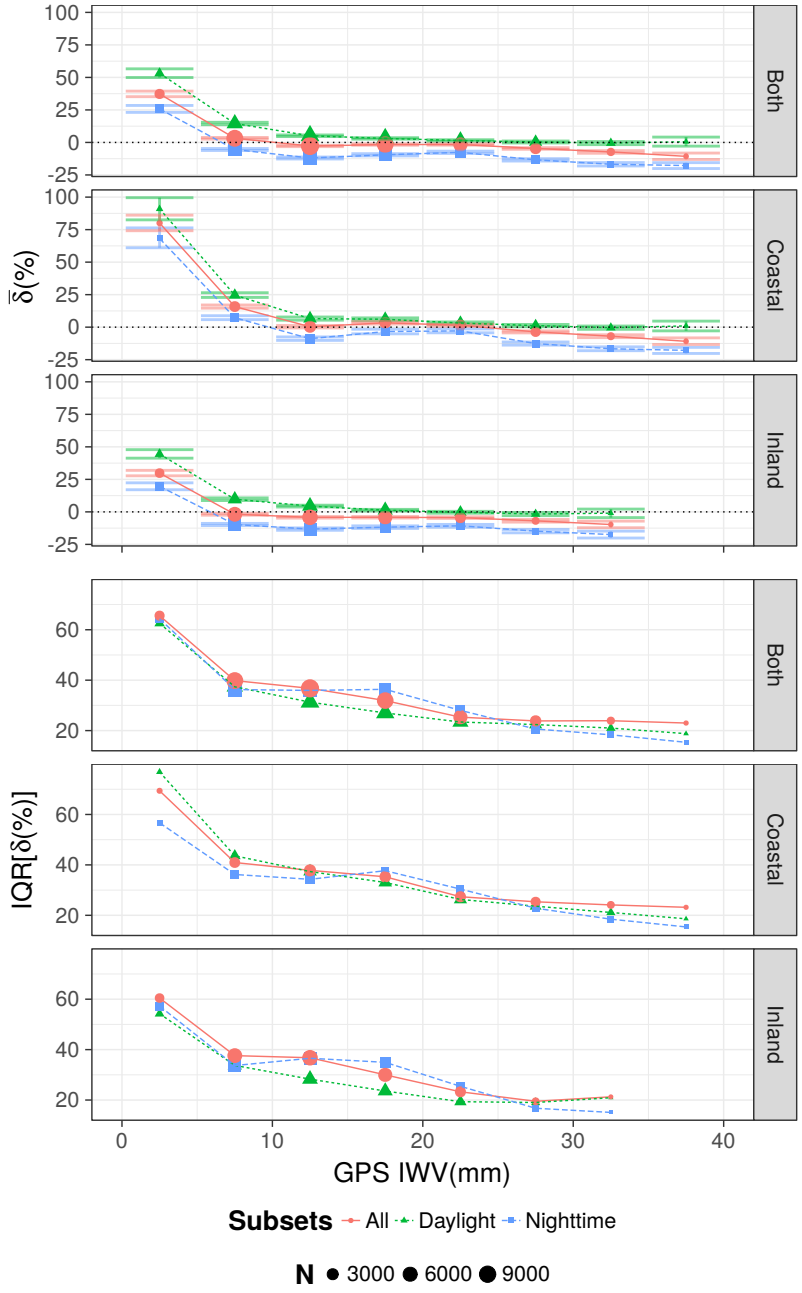

Figure 3: Pseudomedian (top) and IQR (bottom) of MODIS-GPS relative differences as a function of different IWV bins. Error-bars in pseudomedian are the 95% confidence interval in the Wilcoxon rank test.

4.3. SZA dependence

Daylight values can be expected to perform differently for different SZA values, as solar radiation diminishes with increasing SZA. However, nighttime values are not expected to have any difference in performance, except maybe the difference due to the diurnal cycle of IWV and the IWV dependence. Figure 4 top shows the pseudomedian values of MODIS bins against the bin central SZA. It can be observed that MODIS presents a tendency to overestimate IWV for high SZA (SZA $> 50°$) at daytime. A similar behavior was observed in Román et al. (2015) for GOME-2 (visible), and in Vaquero (2017) for OMI (visible). Similarly to OMI behavior, part of MODIS SZA dependence can be explained by variations in the typical IWV for that SZA (diurnal cycle of water vapor). Coastal stations show higher pseudomedian (overestimation) for low IWV subset at daytime. Nighttime values tend to be underestimated, being this underestimation more sensed in inland stations. High IWV tend to be underestimated in most of the SZA range, only overestimated at low SZA values (under 40°), while low IWV tend to be overestimated in the whole range, except for nighttime measurements, from 125° on.

Regarding IQR, Figure 4 shows that, again, daytime values with high SZA ($50° > \text{SZA} > 90°$) present high IQR values for both coastal and inland stations, similarly to GOME-2 behavior in Román et al. (2015) and OMI behavior in Vaquero (2017). Nighttime values are quite stable, with some variability when using high/low IWV separation. Nighttime IQR in coastal stations seems to increase as SZA increases, but this is likely related to the IWV dependence. Around $100° - 125°$, high IWV values are more numerous, and as mentioned above, high IWV values are associated with low IQR values. However, over 125°, low IWV values dominate and thus IQR increases. The dependencies observed for low and high IWV subsets may be related to the fact that after the sunset some sunlight still remains. Generally nighttime IQR is greater than daylight IQR, which is in agreement with Albert et al. (2005); Bennouna et al. (2013).

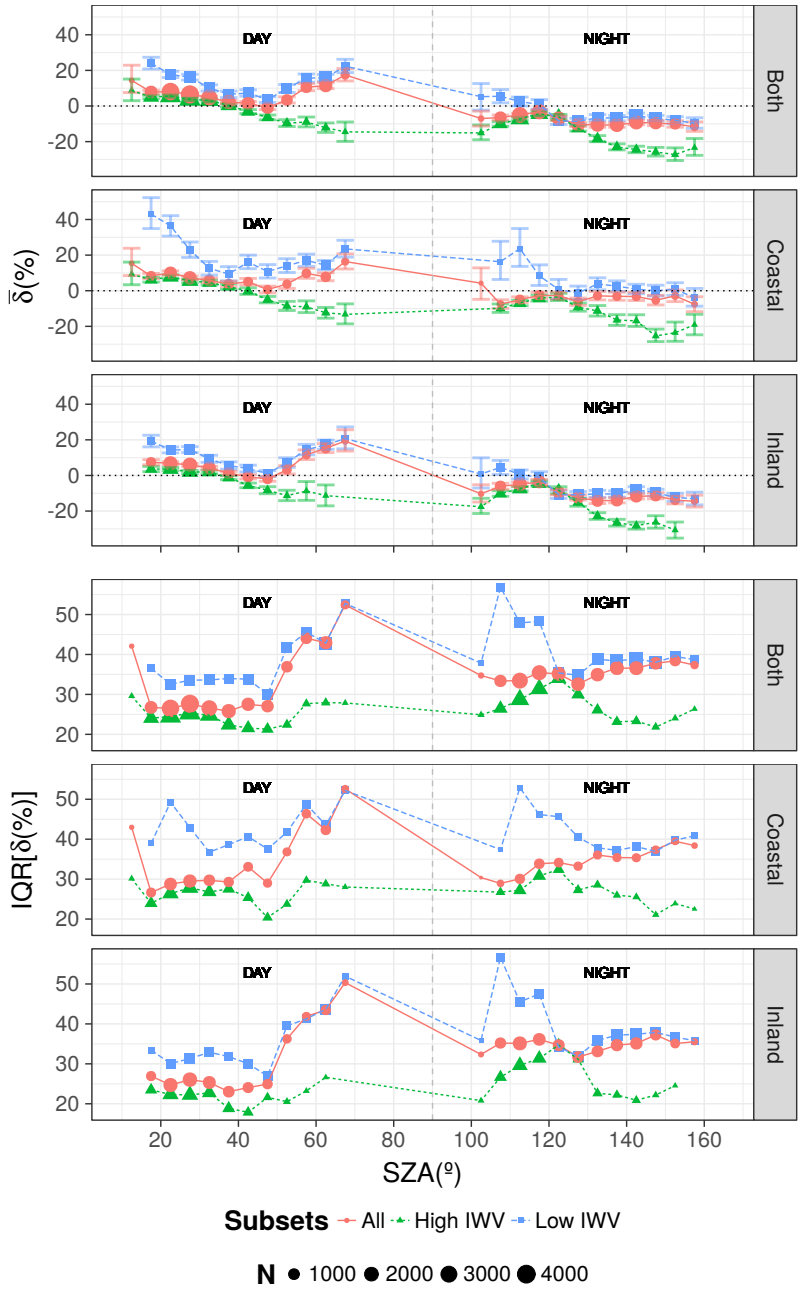

Figure 4: Pseudomedian and IQR of MODIS-GPS relative differences as a function of different IWV bins. Error-bars in pseudomedian are the 95% confidence interval in the Wilcoxon rank test. IWV is considered low if below 14 mm, and high if above 14 mm

4.4. Seasonal dependence

Regarding the seasonal variation of pseudomedian and IQR indices, Figure 5 shows the results of grouping data in bins of 1 month and calculating the pseudomedian and IQR for each bin. Pseudomedian values show overestimation in summer and winter, and underestimation in spring and autumn. This is in agreement with the results in Prasad & Singh (2009); Bennouna et al. (2013). The behavior of the different subsets considered (low/high IWV, daylight and nighttime) is similar, but low IWV and daytime subsets are prone to overestimation while nighttime and high IWV subsets are underestimated. The difference between the two algorithms (daylight and nighttime) agrees with the one observed in Bennouna et al. (2013). Although this behavior is similar to the one observed for OMI in Vaquero (2017) and for AIRS in Raja et al. (2008), in the former work OMI was shown to underestimate during summer, instead of overestimate reference GPS IWV. In the present work, all months are within $\pm$ 30%, except for coastal stations' low IWV subset in summer, which has a exceptionally high overestimation $\sim$ 60%.

The IQR is generally lower in summer than in winter. This is probably due to IWV being typically higher in summer than in winter. Still, coastal summer low IWV is very high (more than 60% in July). It is noticeable that high IWV is very stable. This is similar to the seasonal dependence shown in Vaquero (2017) for OMI, although in the case of OMI IQR values are more extreme, ranging from less than 30% to more than 70%. Nighttime and daytime IQR behave similarly.

4.5. Cloudiness dependence

In order to study cloudiness dependence, cloudy data rejected before are now included in the data set. In Figure 6, data is grouped in bins of 0.1 CF width and the pseudomedian and IQR are represented against CF bins. Pseudomedian is quite stable in the whole CF range. There is a slight tendency to increase overestimation (daylight and low IWV data sets) and underestimation (nighttime and high IWV data sets) as CF increases. Therefore, the treatment of cloud

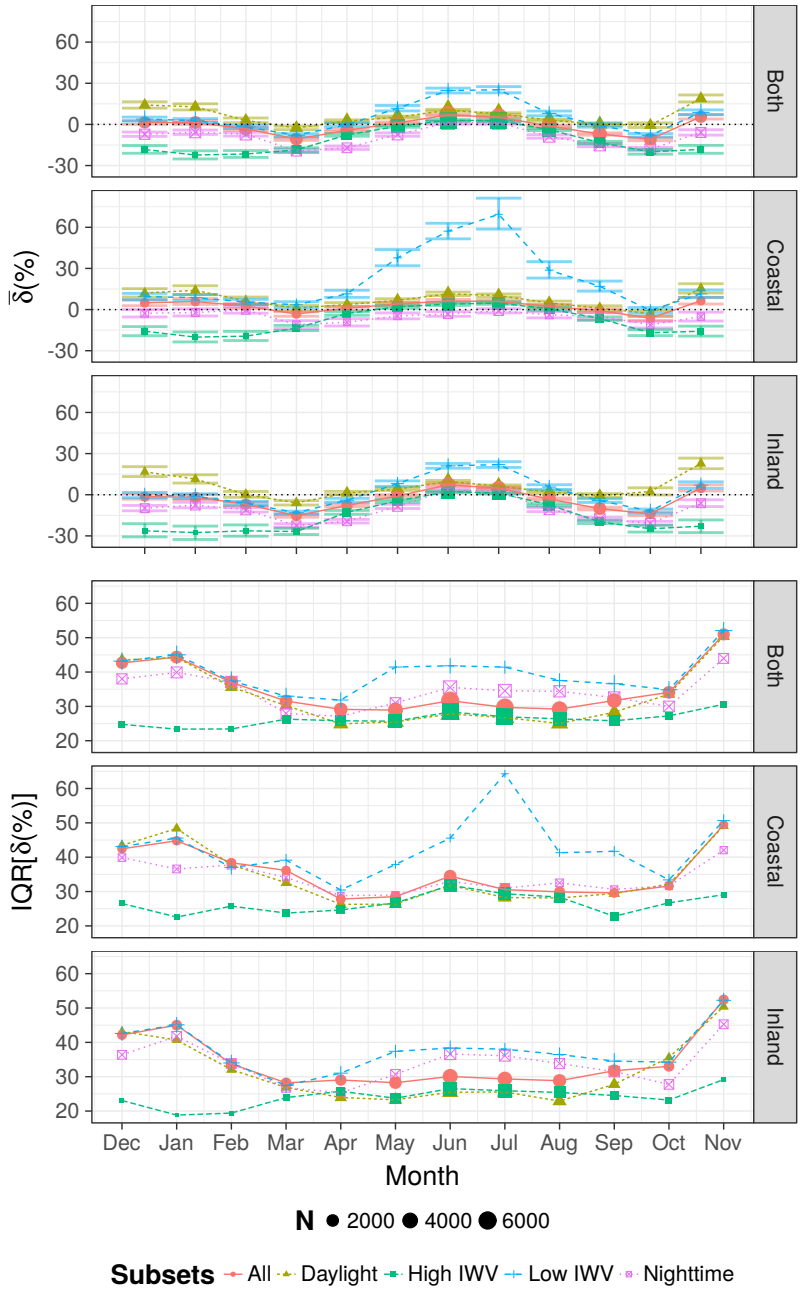

Figure 5: Seasonal dependence on the pseudomedian of MODIS-GPS relative differences. December has been rearranged as the first month in order to make easier to identify the different seasons

scenes in the MODIS retrieval seems to be adequate. Pseudomedian is between $\pm 20\%$ approximately, less than other parameters (IWV or SZA). Cloudy scenes, however, were reported to worsen IWV in Prasad & Singh (2009), where MODIS nighttime measurements are noted to be sensitive only to water vapor above the clouds. Satellite retrievals that do not apply a specific strategy when dealing with cloudy scenes show higher differences (leading to underestimation) when compared against GPS IWV, as shown, for GOME-2 retrieval, in Román et al. (2015).

IQR, however, clearly increases as CF increases. This is expected as clouds add noise to the measurements. Nighttime values are quite stable, due to the use of Earth + atmosphere radiation instead of sunlight. Low IWV values have the highest IQR, probably caused by the fact that a small error in low IWV leads to higher relative errors than in high IWV. Daytime clearly shows a higher IQR (less precision) than nighttime subset.

5. Conclusions

In this work, a validation of MODIS water vapor Level 2 Collection 6 (MOD05_L2 and MYD05_L2) product from the period 2007-2012 in the Iberian Peninsula has been made. MODIS agrees well with GPS ground-based station measurements. However, some dependences have been observed.

IWV dependence is especially important at very low IWV values, where the agreement between MODIS and GPS is not good. MODIS strongly overestimates (pseudomedian around 40%) IWV under 5 mm, with a high variability (IQR around 60%). However, overestimation and variability quickly decrease as IWV increases.

Performance of MODIS water vapor product also varies with SZA. Measurements generally worsen between $50^\circ - 90^\circ$, overestimating low IWV and underestimating high IWV, and increasing IQR. Nighttime measurements (SZA $> 90^\circ$) are quite stable, with a slight tendency to underestimation.

The previous dependences are the cause for a seasonal dependence. Sea-

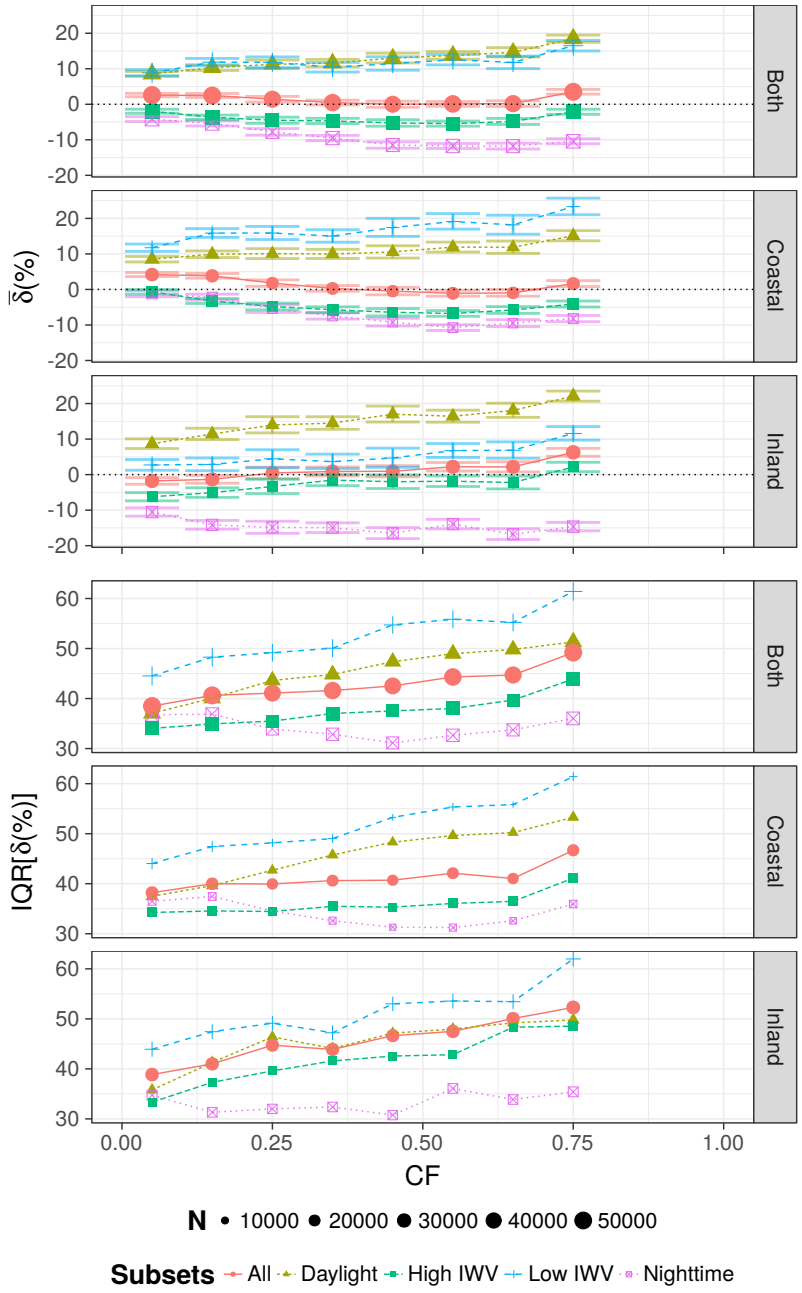

Figure 6: Pseudomedian and IQR of MODIS-GPS relative differences as a function of different CF bins. Errorbars in pseudomedian are the 95% confidence interval in the Wilcoxon rank test.

sonal pseudomedian analysis showed that summer (more daytime hours) and winter (lower IWV) tend to be overestimated, while spring and autumn underestimated. Coastal low IWV subset is overestimated, especially in summer ($\sim 60\%$). IQR is lower in summer and increases in winter. Again, coastal low IWV subset shows high IQR, which is particularly notable in summer ($\sim 60\%$). However, high IWV subset shows very little seasonal dependence.

Finally, all-sky data were considered to study CF dependence. CF has a small influence in the pseudomedian of the relative differences, since positive and negative errors are compensated. Increasing CF worsens subsets (low IWV and daylight by overestimation and high IWV and nighttime by underestimation). Regarding IQR, it increases as CF increases, for all subsets, except nighttime measurements, which are quite stable.

The results in this paper show that the quality of MODIS water vapor product in the Iberian Peninsula is similar to that of other areas. Therefore, this study assures the performance of MODIS in the Iberian Peninsula in terms of the dependence of such performance on several variables. It is expected that this study enables improvements of MODIS NIR and IR algorithms.

Acknowledgments

This work was supported by the Spanish Ministry of Economy and Competitiveness through project CGL2014-56255-C2. Manuel Antón thanks Ministerio de Ciencia e Innovación and Fondo Social (RYC-2011-08345) Europeo for the award of a postdoctoral grant (Ramón y Cajal). Support from the Junta de Extremadura (Research Group Grants GR15137) is gratefully acknowledged. Work at Universidad de Valladolid is supported by project CMT2015-66742-R. Work at Universidad de Granada was supported by the Andalusia Regional Government (project P12-RNM-2409) and the Spanish Ministry of Economy and Competitiveness and FEDER funds under the projects CGL2016-81092-R and "Juan de la Cierva-Formación" program (FJCI-2014-22052). Work at Universidade de Évora is co-funded by the European Union through the Eu-

ropean Regional Development Fund, included in the COMPETE 2020 (Operational Program Competitiveness and Internationalization) through the ICT project (UID / GEO / 04683/2013) with the reference POCI-01-0145-FEDER-007690. The MODIS datasets were acquired from the Level-1 and Atmosphere Archive & Distribution System (LAADS) Distributed Active Archive Center (DAAC), located in the Goddard Space Flight Center in Greenbelt, Maryland (https://ladsweb.nascom.nasa.gov/).

References

Albert, P., Bennartz, R., Preusker, R., Leinweber, R., & Fischer, J. (2005). Remote Sensing of Atmospheric Water Vapor Using the Moderate Resolution Imaging Spectroradiometer. *American Meteorological Society*, *22*, 309–314.

Barnet, C., Manning, E., Rosenkranz, P. W., Strow, L., & Susskind, J. (2007). *Airs-Team Retrieval for Core Products and Geophysical Parameters*. Technical Report March Jet Propulsion Laboratory.

Barreto, A., Cuevas, E., Damiri, B., Romero, P. M., & Almansa, F. (2013). Column water vapor determination in night period with a lunar photometer prototype. *Atmospheric Measurement Techniques*, *6*, 2159–2167. URL: `http://www.atmos-meas-tech.net/6/2159/2013/`. doi:`10.5194/amt-6-2159-2013`.

Bennouna, Y. S., Torres, B., Cachorro, V. E., Ortiz de Galisteo, J. P., & Toledano, C. (2013). The evaluation of the integrated water vapour annual cycle over the Iberian Peninsula from EOS-MODIS against different ground-based techniques. *Quarterly Journal of the Royal Meteorological Society*, *139*, 1935–1956. doi:`10.1002/qj.2080`.

Bevis, M., Businger, S., Herring, T. A., Rocken, C., Anthes, R. A., & Ware, R. H. (1992). GPS Meteorology: Remote Sensing of Atmospheric Water Vapor Using the Global Positioning System. *Journal of Geophys-*

ical Research, *97*, 15787–15801. URL: http://doi.wiley.com/10.1029/92JD01517. doi:10.1029/92JD01517.

Bokoye, A. I., Royer, A., O'Niell, N., Cliche, P., McArthur, L., Teillet, P., Fedosejevs, G., & Thériault, J.-M. (2003). Multisensor analysis of integrated atmospheric water vapor over Canada and Alaska. *Journal of Geophysical Research*, *108*, 21–1 —- 21–16. URL: http://doi.wiley.com/10.1029/2002JD002721. doi:10.1029/2002JD002721.

Chang, L., Gao, G., Jin, S., He, X., Xiao, R., & Guo, L. (2015). Calibration and Evaluation of Precipitable Water Vapor From MODIS Infrared Observations at Night. *IEEE Transactions on Geoscience and Remote Sensing*, *53*, 2612–2620. URL: http://ieeexplore.ieee.org/document/6945895/. doi:10.1109/TGRS.2014.2363089.

Colman, R. (2003). A comparison of climate feedbacks in general circulation models. *Climate Dynamics*, *20*, 865–873. URL: http://link.springer.com/article/10.1007/s00382-003-0310-z. doi:10.1007/s00382-003-0310-z.

Gao, B.-C., & Kaufman, Y. J. (1992). The MODIS Near-IR Water Vapor Algorithm Product ID : MOD05 - Total Precipitable Water. *Algorithm Technical Background Document*, (pp. 1–25). URL: $\delimiter"026E30F$Biblioteca{_}Digital{_}SPR$\delimiter"026E30F$Gao1992{_}ATBD.pdf.

Gao, B.-C., & Li, R.-R. (2008). The Time Series of Terra and Aqua MODIS Near-IR Water Vapor Products. In *IGARSS 2008 - 2008 IEEE International Geoscience and Remote Sensing Symposium* (pp. 186—- 189). IEEE volume 3. URL: http://ieeexplore.ieee.org/document/4779314/. doi:10.1109/IGARSS.2008.4779314.

Grossi, M., Valks, P., Loyola, D., Aberle, B., Slijkhuis, S., Wagner, T., Beirle, S., & Lang, R. (2015). Total column water vapour measurements

from GOME-2 MetOp-A and MetOp-B. *Atmospheric Measurement Techniques*, *8*, 1111–1133. URL: http://www.atmos-meas-tech.net/8/1111/2015/. doi:10.5194/amt-8-1111-2015.

de Haan, S., van der Marel, H., & Barlag, S. (2002). Comparison of GPS slant delay measurements to a numerical model: case study of a cold front passage. *Physics and Chemistry of the Earth, Parts A/B/C*, *27*, 317–322. URL: http://linkinghub.elsevier.com/retrieve/pii/S1474706502000062. doi:10.1016/S1474-7065(02)00006-2.

Heise, S., Dick, G., Gendt, G., Schmidt, T., & Wickert, J. (2009). Integrated water vapor from IGS ground-based GPS observations: initial results from a global 5-min data set. *Annales Geophysicae*, *27*, 2851–2859. URL: http://www.ann-geophys.net/27/2851/2009/. doi:10.5194/angeo-27-2851-2009.

Ichoku, C., Levy, R., Kaufman, Y. J., Remer, L. A., Li, R.-R., Martins, V. J., Holben, B. N., Abuhassan, N., Slutsker, I., Eck, T. F., & Pietras, C. (2002). Analysis of the performance characteristics of the five-channel Microtops II Sun photometer for measuring aerosol optical thickness and precipitable water vapor. *Journal of Geophysical Research*, *107*, 5–1—- 5–17. URL: http://doi.wiley.com/10.1029/2001JD001302. doi:10.1029/2001JD001302.

King, M., Kaufman, Y., Menzel, W., & Tanre, D. (1992). Remote sensing of cloud, aerosol, and water vapor properties from the moderate resolution imaging spectrometer (MODIS). *IEEE Transactions on Geoscience and Remote Sensing*, *30*, 2–27. URL: http://ieeexplore.ieee.org/document/124212/. doi:10.1109/36.124212.

Li, Z., Muller, J.-P., & Cross, P. (2003). Comparison of precipitable water vapor derived from radiosonde, GPS, and Moderate-Resolution Imaging Spectroradiometer measurements. *Journal of Geophysical Research*, *108*, 4651. URL: http://doi.wiley.com/10.1029/2003JD003372. doi:10.1029/2003JD003372.

Livesey, N. J., & Van Snyder, W. (2004). *EOS MLS Retrieval Processes Algorithm Theoretical Basis*. Technical Report part 3 Jet Propulsion Laboratory.

Martinez, M. A. (2013). *Algorithm Theoretical Basis Document for "SEVIRI Physical Retrieval Product" (SPhR-PGE13 v2.0)*. Technical Report Agencia Estatal de Meteorología (AEMET). URL: `http://www.nwcsaf.org/scidocs/Documentation/SAF-NWC-CDOP2-INM-SCI-ATBD-13{_}v2.0.pdf`.

Myhre, G., Shindell, D., Bréon, F.-M., Collins, W., Fuglestvedt, J., Huang, J., Koch, D., Lamarque, J.-F., Lee, D., Mendoza, B., Nakajima, T., Robock, A., Stephens, G., Takemura, T., & Zhang, H. (2013). Anthropogenic and Natural Radiative Forcing. In *Climate Change 2013: The Physical Science Basis. Contribution of Working Group I to the Fifth Assessment Report of the Intergovernmental Panel on Climate Change* (pp. 659–740).

Niell, A. E. (2000). Improved atmospheric mapping functions for VLBI and GPS. *Earth, Planets and Space*, *52*, 699–702. URL: `http://earth-planets-space.springeropen.com/articles/10.1186/BF03352267`. doi:`10.1186/BF03352267`.

Ningombam, S. S., Jade, S., Shrungeshwara, T., & Song, H.-J. (2016). Validation of water vapor retrieval from Moderate Resolution Imaging Spectroradiometer (MODIS) in near infrared channels using GPS data over IAO-Hanle, in the trans-Himalayan region. *Journal of Atmospheric and Solar-Terrestrial Physics*, *137*, 76–85. URL: `http://linkinghub.elsevier.com/retrieve/pii/S1364682615301000`. doi:`10.1016/j.jastp.2015.11.019`.

Noël, S., Buchwitz, M., & Burrows, J. P. (2004). First retrieval of global water vapour column amounts from SCIAMACHY measurements. *Atmospheric Chemistry and Physics*, *4*, 111–125. URL: `http://www.atmos-chem-phys.net/4/111/2004/`. doi:`10.5194/acp-4-111-2004`.

Ohtani, R., & Naito, I. (2000). Comparisons of GPS-derived precipitable water vapors with radiosonde observations in Japan. *Journal of Geophysical Re-*

search: Atmospheres, *105*, 26917–26929. URL: http://doi.wiley.com/10.1029/2000JD900362. doi:10.1029/2000JD900362.

Ortiz de Galisteo, J. P., Bennouna, Y., Toledano, C., Cachorro, V., Romero, P., Andrés, M. I., & Torres, B. (2014). Analysis of the annual cycle of the precipitable water vapour over Spain from 10-year homogenized series of GPS data. *Quarterly Journal of the Royal Meteorological Society*, *140*, 397–406. URL: http://doi.wiley.com/10.1002/qj.2146. doi:10.1002/qj.2146.

Ortiz de Galisteo, J. P., Cachorro, V., Toledano, C., Torres, B., Laulainen, N., Bennouna, Y., & de Frutos, A. (2011). Diurnal cycle of precipitable water vapor over Spain. *Quarterly Journal of the Royal Meteorological Society*, *137*, 948–958. doi:10.1002/qj.811.

Pany, T., Pesec, P., & Stangl, G. (2001). Atmospheric GPS slant path delays and ray tracing through numerical weather models, a comparison. *Physics and Chemistry of the Earth, Part A: Solid Earth and Geodesy*, *26*, 183–188. URL: http://linkinghub.elsevier.com/retrieve/pii/S1464189501000448. doi:10.1016/S1464-1895(01)00044-8.

Pérez-Ramírez, D., Navas-Guzmán, F., Lyamani, H., Fernández-Gálvez, J., Olmo, F. J., & Alados-Arboledas, L. (2012). Retrievals of precipitable water vapor using star photometry: Assessment with Raman lidar and link to sun photometry. *Journal of Geophysical Research: Atmospheres*, *117*, n/a–n/a. URL: http://doi.wiley.com/10.1029/2011JD016450. doi:10.1029/2011JD016450.

Prasad, A. K., & Singh, R. P. (2009). Validation of MODIS Terra, AIRS, NCEP/DOE AMIP-II Reanalysis-2, and AERONET Sun photometer derived integrated precipitable water vapor using ground-based GPS receivers over India. *Journal of Geophysical Research*, *114*, D05107. URL: http://doi.wiley.com/10.1029/2008JD011230. doi:10.1029/2008JD011230.

Raja, M. K. R. V., Gutman, S. I., Yoe, J. G., McMillin, L. M., & Zhao, J. (2008). The Validation of AIRS Retrievals of Integrated Precipitable Water

Vapor Using Measurements from a Network of Ground-Based GPS Receivers over the Contiguous United States. *Journal of Atmospheric and Oceanic Technology*, *25*, 416–428. URL: http://journals.ametsoc.org/doi/abs/10.1175/2007JTECHA889.1. doi:10.1175/2007JTECHA889.1.

Román, R., Antón, M., Cachorro, V., Loyola, D., Ortiz de Galisteo, J., de Frutos, A., & Romero-Campos, P. (2015). Comparison of total water vapor column from GOME-2 on MetOp-A against ground-based GPS measurements at the Iberian Peninsula. *Science of The Total Environment*, *533*, 317–328. URL: http://dx.doi.org/10.1016/j.scitoenv.2015.06.124http://linkinghub.elsevier.com/retrieve/pii/S0048969715303260. doi:10.1016/j.scitotenv.2015.06.124.

Román, R., Bilbao, J., & de Miguel, A. (2014). Uncertainty and variability in satellite-based water vapor column, aerosol optical depth and Angström exponent, and its effect on radiative transfer simulations in the Iberian Peninsula. *Atmospheric Environment*, *89*, 556–569. URL: http://dx.doi.org/10.1016/j.atmosenv.2014.02.027http://linkinghub.elsevier.com/retrieve/pii/S135223101400123X. doi:10.1016/j.atmosenv.2014.02.027.

Salomonson, V., Barnes, W., Maymon, P., Montgomery, H., & Ostrow, H. (1989). MODIS: advanced facility instrument for studies of the Earth as a system. *IEEE Transactions on Geoscience and Remote Sensing*, *27*, 145–153. URL: http://ieeexplore.ieee.org/document/20292/. doi:10.1109/36.20292.

Schneider, M., Romero, P. M., Hase, F., Blumenstock, T., Cuevas, E., & Ramos, R. (2010). Continuous quality assessment of atmospheric water vapour measurement techniques: FTIR, Cimel, MFRSR, GPS, and Vaisala RS92. *Atmospheric Measurement Techniques*, *3*, 323–338. URL: http://www.atmos-meas-tech.net/3/323/2010/. doi:10.5194/amt-3-323-2010.

Schroedter-Homscheidt, M., Drews, A., & Heise, S. (2008). Total water vapor

column retrieval from MSG-SEVIRI split window measurements exploiting the daily cycle of land surface temperatures. *Remote Sensing of Environment*, *112*, 249–258. URL: http://linkinghub.elsevier.com/retrieve/pii/S0034425707001952. doi:10.1016/j.rse.2007.05.006.

Seemann, S. W., Borbas, E. E., Li, J., Menzel, W. P., & Gumley, L. E. (2006). *Modis Atmospheric Profile Retrieval: Algorithm Theoretical Basis Document*. Technical Report October Cooperative Institute for Meteorological Satellite Studies, University of Wisconsin-Madison. URL: $\delimiter"026E30F$Biblioteca{_}Digital{_}SPR$\delimiter"026E30F$Seemann2006{_}ATBD.pdf.

Torres, B., Cachorro, V. E., Toledano, C., Ortiz de Galisteo, J. P., Berjón, A., de Frutos, A. M., Bennouna, Y., & Laulainen, N. (2010). Precipitable water vapor characterization in the Gulf of Cadiz region (southwestern Spain) based on Sun photometer, GPS, and radiosonde data. *Journal of Geophysical Research*, *115*, 1–11. URL: http://doi.wiley.com/10.1029/2009JD012724. doi:10.1029/2009JD012724.

Turner, D. D., Clough, S. A., Liljegren, J. C., Clothiaux, E. E., Cady-Pereira, K. E., & Gaustad, K. L. (2007). Retrieving Liquid Wat0er Path and Precipitable Water Vapor From the Atmospheric Radiation Measurement (ARM) Microwave Radiometers. *IEEE Transactions on Geoscience and Remote Sensing*, *45*, 3680–3690. URL: http://ieeexplore.ieee.org/document/4373386/. doi:10.1109/TGRS.2007.903703.

Turner, D. D., Ferrare, R. A., Brasseur, L. A. H., Feltz, W. F., & Tooman, T. P. (2002). Automated Retrievals of Water Vapor and Aerosol Profiles from an Operational Raman Lidar. *Journal of Atmospheric and Oceanic Technology*, *19*, 37–50. URL: http://journals.ametsoc.org/doi/abs/10.1175/1520-0426{%}282002{%}29019{%}3C0037{%}3AAROWVA{%}3E2.0.CO{%}3B2. doi:10.1175/1520-0426(2002)019<0037:AROWVA>2.0.CO;2.

Vaquero, J. M. (2017). Ball lightning: a Renaissance account from Zafra

(Spain). *History of Geo- and Space Sciences*, *8*, 53–56. URL: http://www.hist-geo-space-sci.net/8/53/2017/. doi:10.5194/hgss-8-53-2017.

Vaquero-Martínez, J., Antón, M., Ortiz de Galisteo, J. P., Cachorro, V. E., Wang, H., González Abad, G., Román, R., & Costa, M. J. (2017). Validation of integrated water vapor from OMI satellite instrument against reference GPS data at the Iberian Peninsula. *Science of The Total Environment*, *580*, 857–864. URL: http://linkinghub.elsevier.com/retrieve/pii/S0048969716327176. doi:10.1016/j.scitotenv.2016.12.032.

Wang, H., Liu, X., Chance, K., González Abad, G., & Chan Miller, C. (2014). Water vapor retrieval from OMI visible spectra. *Atmospheric Measurement Techniques*, *7*, 1901–1913. URL: http://www.atmos-meas-tech.net/7/1901/2014/. doi:10.5194/amt-7-1901-2014.

Wang, J., Zhang, L., Dai, A., Van Hove, T., & Van Baelen, J. (2007). A near-global, 2-hourly data set of atmospheric precipitable water from ground-based GPS measurements. *Journal of Geophysical Research*, *112*, D11107. URL: http://doi.wiley.com/10.1029/2006JD007529. doi:10.1029/2006JD007529.

Wentz, F. J., & Meissner, T. (2007). *Supplement 1 Algorithm Theoretical Basis Document for AMSR-E Ocean Algorithms*. Technical Report .

Wentz, F. J., & Spencer, R. W. (1998). SSM/I Rain Retrievals within a Unified All-Weather Ocean Algorithm. *Journal of the Atmospheric Sciences*, *55*, 1613–1627. URL: http://journals.ametsoc.org/doi/abs/10.1175/1520-0469{%}281998{%}29055{%}3C1613{%}3ASIRRWA{%}3E2.0.CO{%}3B2. doi:10.1175/1520-0469(1998)055<1613:SIRRWA>2.0.CO;2.

Wilcoxon, F. (1945). Individual Comparisons by Ranking Methods. *Biometrics Bulletin*, *1*, 80. URL: http://www.jstor.org/stable/10.2307/3001968?origin=crossref. doi:10.2307/3001968.